PCCP

Accepted Manuscript

ROYAL SOCIETY OF CHEMISTRY

www.rsc.org/pccp

Journal Name

RSCPublishing

ARTICLE

New organophilic kaolin clays based on single- point grafted 3-aminopropyl dimetylethoxysilane†

Cite this: DOI: 10.1039/xoxxoooooox

A. Zaharia,[a] F.-X. Perrin,*[b] M. Teodorescu,[c] A.-L. Radu,[a] T.-V. Iordache,[a] A.-M. Florea,[a] D. Donescu,[a] and A. Sarbu,*[a]

Received ooth January 2012,
Accepted ooth January 2012

DOI: 10.1039/xoxxoooooox

www.rsc.org/

In this study is depicted for the first time the organophilization procedure of kaolin rocks with a monofunctional ethoxysilane - 3 aminopropyl dimethyl ethoxysilane (APMS). The two-step organophilization procedure, e.g. dimethyl sulfoxide intercalation and APMS grafting onto the inner hydroxyl surface of kaolinite (the mineral) layers was tested for three sources of Kaolin rocks (KR, KC and KD) with various morphologies and kaolinite compositions. The load of APMS in the kaolinite interlayer space was higher than that of 3-aminopropyl triethoxysilane (APTS) due to the single-point grafting nature of the organophilization reaction. A higher long-distance order of kaolinite layers with low staking was obtained for the APMS thereof, due to a more controllable organiphilization reaction. Last but not least, the solid state ^{29}Si-NMR tests confirmed the single-point grafting mechanism of APMS, corroborating a monodentate fixation on the kaolinite hydroxyl facet, with no contribution to the bidentate or the tridentate fixation as observed for APTS.

Introduction

The inorganic-organic materials form nowadays are an intensely researched class of materials with quite remarkable properties, which rely on the nano-scale incorporation of the filler into the organic matrix.[1-4] From this point of view, clay-type fillers are maybe the most studied. Both the clay incorporation and the properties of the resulting material strongly depend on the compatibility between the clay and the organic matrix. The incompatibility between hydrophilic layered aluminosilicates and the organophilic polymer has been solved through surface modification of the clays.[5,6] This is usually done via a reaction of the clay surface with organics producing organically-modified layered aluminosilicates. The modified surfaces have the role to expand the interlayer space of clay, thus facilitating the penetration of polymer. A number of such studies on the intercalated materials have been reported using different ceramic phases in connection with a variety of polymers.[7-12]

Kaolinite is a hydrous aluminum silicate mineral with good physical properties and stable chemical structure found in kaolin rocks. It is a very important non-metallic material, representing the base material for the ceramics, chemical engineering, plastics, paint and fire-resistant materials industries due to its excellent characteristic. Kaolinite structure can be described as a 1:1 sheet structure composed of SiO_4 tetrahedral layers and $Al(O,OH)_6$ octahedral layers.[13] The morphology of the kaolinite particle has the shape of a hexagonal plate. An individual kaolinite layer has an oxygen surface on one side and a hydroxyl surface on the other, through which it is strongly hydrogen bonded to the platelets above and below it. These hydrogen and Van der Waals bonds make the intercalation process more difficult than for other clays, as for instance montmorillonite, vermiculite, etc.[5,13,14] Kaolinite is known as hydrophilic clay, leading to better particles dispersion in the aqueous applications. For non-aqueous applications, the kaolinite particles require a surface treatment for improving the compatibility with the organic matrix.[15] Hydrogen bonds between the layers also generate a very small interlayer space, which allow only a limited number of small polar guest molecules (such as dimethyl sulfoxide

[a] Advanced Polymer Materials and Polymer Recycling Group
The National R&D Institute for Chemistry and Petrochemistry ICECHIM
Splaiul Independentei 202, 060021, Bucharest, Romania
*E-mail: andr.sarbu@gmail.com
[b] Laboratoire Matériaux Polymères Interfaces et Environnement Marin
Universite du Sud Toulon-Var
BP 132, 83957 La Garde Cedex, France
*E-mail: perrin@univ-tln.fr
[c] Department of Bioresources and Polymer Science
Politehnica University of Bucharest
Calea Victoriei 149, 010072 Bucharest, Romania

(DMSO), N-methyl formamide, urea) to be directly intercalated.[6,16-18] The guest molecules are intercalated through the formation of new hydrogen bonds; hence, this displacement method yields various intercalated compounds. For example, the intercalation compounds with methanol were mostly used as intermediates for guest displacement reaction.[19-21] Detellier and co-workers also obtained various kaolinite hybrids. For this matter, DMSO-kaolinite intercalates were prepared in order to increase the interlayer space and to make it accessible for further organic chemical grafting.[22-25]

The present paper aimed at studying the behavior of some commercial kaolin samples from different sources, with various morphologies and kaolinite compositions, in the organophilization reaction with the targeted monofunctional organosilane. To the best of our knowledge[26,27], kaolinite organophilization with a monofunctional aminosilane is being reported for the first time in this paper. Our newest findings were compared with those obtained with a trifunctional organosilane, the common grafting agent presented in several literature studies[28,29,30]. For this matter, a Romanian (KR) and two Brazilian (kaolin-C, KC, and kaolin-D, KD) types of commercial kaolin were used for the organophilization reaction with 3 aminopropyl dimethyl ethoxysilane (APMS) – the monofunctional silane and 3 aminopropyl triethoxysilane (APTS) – the trifunctional silane (**Fig S1, ESI)**. Ethoxysilanes with amino groups were selected due to their specific properties, which can further allow the modified kaolinite to be used as a reinforcing agent in various mixtures (e.g. as reinforcing agents for various polymers with complementary functionalities).

Results and Discussion

Theoretical Approach

For achieving a successful organophilization reaction, the intercalation step with dimethyl sulfoxide (DMSO) molecules was necessary in order to enlarge the interlayer space of kaolinite. Although, kaolinite modification with trifunctional aminosilanes was extensively studied and described in the literature,[28,29,30] APTS grafting was also performed using the same conditions as for APMS grafting, in order to highlight the new findings properly.

The main reason for employing monoethoxysilane refers to several advantages over the use of triethoxysilane: i) the monoethoxysilane molecule is somewhat smaller (due to the replacement of two ethoxy groups by two methyl groups) allowing an easier penetration of the kaolin interlayer space; and ii) the monofunctional ethoxysilane has only one anchoring group (i.e. the ethoxy group), which allows the formation of a single bond with only one kaolin layer, unlike triethoxysilane that, may react with two different platelets in the presence of water traces, leading to interconnected structures (as suggested by Avila and co-workers[29] for kaolin and by Gianni and co-workers[31] for montmorillonite). In such situation it is obvious that exfoliation or an increase of the interlayer distance, are not further possible. Additionally, the bridging reaction of layers caused by trifunctional aminosilanes can be responsible for diminishing the interlayer space gained during DMSO pre-intercalation.

Raw kaolin

Morphology. The SEM analysis (**Fig 1** A and B) clearly showed strong morphological differences among the three raw kaolin samples. KR and KC consisted of small irregular-shaped particles (<6 μm). High aggregation degrees were observed especially for KR (over 60 μm large), while KD was composed of big spherical particles, within 5-25 μm size range (**Fig 1** C). The micrographs also revealed more porous surface structures for KR and KC samples relative to KD, which can provide an easier access of reactants in the interlayer space of kaolinite and implicitly higher intercalation yields.

Fig 1 Shape and morphology of the raw kaolin samples KR (A), KC (B) and KD (C).

Thermal analyses and composition. The values of oxide residues (**Table 1**) at 1000°C were in agreement, particularly for KC and KD, with the oxide content determined by EDAX analyses (**Table 1**).

Table 1 The effective kaolinite content of each kaolin sample based on EDAX results

Not	k[a]	K_{EDAX}[a]	K'_{EDAX}[a]	R[b]	PW[b]	K'_{TGA}[b]	K_{TGA}[b]
KR	99.91	91.2	103.97	92.0	5.4	38.5	33.1
KC	87.01	85.4	97.36	86.5	13.98	97.22	83.24
KD	87.24	84.0	95.76	86.7	13.70	95.27	81.57

[a] whereas k= kaolin oxide content and K_{EDAX}=Kaolinite oxide content (SiO_2+ Al_2O_3) were given by EDAX; and, K'_{EDAX}= effective Kaolinite extent was calculated by summing the K_{EDAX} value and the theoretical water content (T_w) determined according to the specific reaction of kaolinite conversion into *m*-kaolinite as 12.77 wt% for KR, 11.96 wt% for KC and 11.76 wt% for KD;

[b] whereas R=Oxide residues and PW= practical water loss were given by TGA; K'_{TGA}= effective Kaolinite extent was further calculated using the equation: $K'_{TGA}= PW \cdot K'_{EDAX}/T_w$; and K_{TGA}= Kaolinite oxide content (SiO_2+ Al_2O_3) was calculated by removing the water loss PW;

TGA corroborated with DTG (**Fig S2, ESI**) can elucidate the inconsistency between KR compositions (**Table 1**) determined by the two methods. The theoretical mass loss during kaolinite [$Al_2Si_2O_5(OH)_4$] conversion to *m*-kaolinite [$Al_2Si_2O_7$] is about 14 wt % relative to kaolinite, according to the specific reaction: $Al_2Si_2O_5(OH)_4 \Rightarrow Al_2Si_2O_7 + 2x\ H_2O$. Implicitly, a theoretical water content of 12.77 wt% for KR, 11.96 wt% for KC and 11.76 wt% for KD (calculated relative to the oxide content of SiO_2 and Al_2O_3 given by EDAX, **Table 1**) should have been registered. But when calculating the effective kaolinite content of each sample (**Table 1**) based on EDAX results, the value for KR type turned inconclusive. This happened because the effective content of kaolinite in KR corresponded to the 5.4 wt% mass loss (characteristic for *m*-

kaolinite formation) instead of the theoretical 12.77 %, meaning approximately 38.5% (or 33.1% relative to oxides residues given by TGA). Consequently, higher oxide extents within KR and decreased mass loss during kaolinite dehydroxylation indicated the presence of considerable heterogeneous phases within kaolin particles. Hence, the remaining residues of KR, KC and KD (i.e. 58.9%, 3.26% and 5.13% respectively) relative to the oxide residues represented heterogeneous oxide phases within kaolin rocks.

Still, EDAX results indicated higher oxide content in KR, compared to the oxide residues determined by TGA. This particular inconsistency was due to the fact that EDAX is a surface analyse technique, giving appropriate values for the oxide content on the upper layers of kaolin particles. Correlating TGA that indicated the presence of increased contents of heterogeneous phases, with EDAX measurements, it can be supposed that the kaolinite structures are likely to be the core of the particles, while the heterogeneous oxide phases are peripheral. This hypothesis can also explain gibbsite transformation in boehmite, in KR, by creating favourable conditions. According to Frost *et. all,*[32] gibbsite [γ-$Al(OH)_3$] decomposes through the intermediary form of boehmite structure [γ-AlOOH] in hydrothermal conditions, meaning slow rates of water loss due to structure related factors like size of aggregates and location of water content. In this context, the morphology of KR, with regard to particle size, also sustained the creation of a hydrothermal environment. Thus, the boehmite content formed during gibbsite dehydration added up to the existing one in KR, being further transformed into Al_2O_3.

On the other hand, for purer KC and KD, degradation occurred in a single step, characteristic to kaolinite dehydroxylation, recorded at 515°C and at 495°C, respectively. The total water loss of about 14 % registered for these two kaolin rock types approached the theoretical mass loss during conversion to *m*-kaolinite and the effective kaolinite content (**Table 1**) was similar for both TGA and EDAX.

It has been previously shown that the degree of kaolin crystallinity is directly related to its thermal stability. As a result, kaolin samples with lower concentrations of defects (heterogeneous phases) are more thermally stable and dehydroxylation of kaolinite occurs at higher temperatures.[32] Therefore, based on the TGA/DTG analyses, it can be noted that KC and KD samples were purer than KR while the content of crystal defects decreased in the following order KR>KD>KC[4].

Structure. The FTIR spectra of KR, KC and KD (**Fig S3** a and b, **ESI**) were similar, and agreed well with those reported in the literature.[33,34,35] KR spectrum displays three additional bands at 3520, 3450 and 3360 cm^{-1} corresponding to the polycrystalline gibbsite as revealed by TGA also.

XRD patterns of kaolin powder types are given in the **ESI**, see **Fig S4**. All samples displayed characteristic basal diffraction peaks at 7.1 Å and 3.5 Å, as literature reports.[36,37] The XRD spectra also enabled the qualitative evaluation of purity for employed kaolin samples. Hence, the presence of several impure phases within the KR powder, i.e. potassium aluminium silicate (KAlSi), gibbsite (G, $Al(OH)_3$), and quartz (Q, (SiO_2)) were noticed, while the XRD spectra of both Brazilian kaolin samples, KD and KC, were close to pure kaolinite.[36,37] The pattern of KC and KD in the 19-23.5° 2θ region was typical for well-ordered kaolinite,[36] while that observed for KR was characteristic to a more disordered structure; thus, being consistent with the TGA observations.

DMSO -kaolinite intercalation

Thermal analyses and composition. In addition to characteristic decomposition steps of raw kaolin,[38] the TGA/DTG curves (**Fig S5, ESI**) of the three DMSO-intercalated kaolin samples registered the first weight loss around 155°C, ascribed to DMSO decomposition.[39] This additional degradation step indicated the presence of DMSO molecules within kaolin structure (in accordance with XRD observation).

The amount of DMSO incorporated into kaolin is very low for KD type, about 2%, which can be the result of the confined spherical morphology and high particle size. However, the amount of DMSO, incorporated into KC and KR kaolin types was about 21 wt% (or 21.1 wt% relative to the effective kaolinite) and 5 wt% (or 19.2 wt% relative to effective kaolinite), respectively. Accepting the fact that more than 60% of KR is constituted from heterogeneous phases, the ratio of DMSO relative to the effective kaolinite was similar to that of KC. Nevertheless, the results obtained for the KC type agrees more with the literature data available for the intercalation process with DMSO. It can also be noted that the increased amount of intercalated DMSO within KC and KR kaolinite structure was related to the morphology of powder. In both cases, smaller size of aggregates provided an increased surface area and more access points for DMSO diffusion into the interlamellar space. Altogether, the specific surface area which increases in the KD < KR < KC order seems to be the main factor in determining the amount of DMSO incorporated into kaolinite. It is also possible, that the disorder increase in the KR<KD<KC order to be an additional factor for the efficiency of DMSO intercalation, as shown by others.[40]

Structure. Compared to FTIR spectrum of KC alone, KC-DMSO (**Fig S6** a and b, **ESI**) reveals new bands at 3540 and 3500 cm^{-1} (ν_{OH}) assigned to water- DMSO interactions occurring within the kaolinite interlayer space.[41,42] New bands appeared for KR-DMSO as well, overlapping with the characteristic ν_{OH} bands of gibbsite, and the stretching vibrations related to the inner hydroxyl surface were affected by the guest molecules. For instance, the intensity decrease of the 3695 cm^{-1} band, registered for KC- and KR- DMSO thereof, was the result of S=O interactions with the interlamellar hydroxyl groups which generated multiple hydrogen bonds[42] New bands, i.e. 3020 cm^{-1} and 2930 cm^{-1}, corresponding to ν_{CH3} reflected the presence of DMSO molecules in KC-DMSO and KR-DMSO samples (**Fig S6**a).[16,21,22-29] Furthermore, the

shifting of Al-OH_{inter} characteristic band from 938 cm^{-1} to 958 cm^{-1}, in KC-DMSO and KR-DMSO was due to hydroxyl (aluminol)-methyl (DMSO) interactions (**Fig S6**b); and, the shifting of the 914 cm^{-1} band (in raw kaolin) to 905 cm^{-1} was associated to the repulsive interaction between methyl groups of DMSO with the hydroxyl surface of kaolinite layers.[33,43] Consequently, bands displacement, assigned to intermolecular interactions, sustained the DMSO intercalation process. Together with the TGA results, FTIR provided further evidence referring to the successful DMSO intercalation for KC and KR.

XRD patterns of the intercalated kaolin samples are shown in **Fig S7, ESI**. The 001 reflection of KC and KR appears shifted towards higher spacing (i.e. 10.9 Å), supporting the intercalation of DMSO between the clay layers. The intercalation process with DMSO molecules practically did not take place within KD structure. This assumption was indicated by the presence of a more intense d_{001} peak characteristic for unmodified KD at 7.1 Å relative to the d_{001} peak characteristic for intercalated KD at 10.9 Å.

The next organophilization step was performed only for KC-DMSO and KR-DMSO where DMSO was successfully intercalated.

Organophilization process

Thermal analyses and composition. KC-APTS and KC-APMS displayed two degradation steps (**Fig 2**).

Fig 2 TGA curves and DTG inset of KC thereof; raw kaolin sample (KC), DMSO-intercalate (KC-DMSO), and organophilized samples with APMS and APTS (KC-APMS and KC-APTS).

The first weight loss occurred at a maximum decomposition temperature of 235°C for KC-APTS and of 295°C for KC-APMS, respectively; both being much higher than that registered for KC-DMSO (i.e. 180°C). This supports the functionalization of kaolinite with aminosilane. No significant weight loss was observed within the 170-210°C interval, meaning that DMSO molecules were either replaced by APTS or APMS molecules or simply removed within the kaolinite interlamellar space during the silanization process. However, the broad decomposition range of silane, starting from about 170°C can mask possible traces of DMSO remaining in the interlamellar space. The second step ranged between 400°C and 650°C and corresponded entirely to clay dehydroxylation as indicated by the expected mass loss. It is noteworthy the fact that the maximum degradation temperatures of silanized kaolinite (i.e. 493°C for KC-APTS and 487°C for KC-APMS, respectively) were inferior to those of KC alone (515 ^{O}C). These results were consistent with other literature observations referring to the influence of trifunctional silane molecules upon the phase change from kaolinite to *m*-kaolinite.[29] Taking into account the mass loss from TGA and considering the fact that the first step was related only to the hydrocarbon fraction of fully condensed silane, the formulas of KC thereof can be calculated as follows: $Al_2Si_2O_5(OH)_4 \cdot (NH_2(CH_2)_3SiO_{1,5})_{0.22}$ for KC-APTS, and $Al_2Si_2O_5(OH)_4 \cdot (NH_2(CH_2)_3Si(CH_3)_2O)_{0.33}$ for KC-APMS, respectively.

The thermal behaviour of the organophilized KR indicated a complex weight loss (**Fig 3**), related to the presence of predominant heterogeneous oxide phases, other than kaolinite. Some traces of DMSO were still present here and masked by the first mass loss around 180°C, the one assigned to bonded water in the raw KR. The following degradation steps, recorded within 250-300°C and 300-515°C temperature ranges were assigned to dehydration of gibbsite and degradation of the hydrocarbon fraction of silane, respectively. For the latter, the maximum decomposition temperatures were shifted towards higher values compared to the DMSO-intercalated structures. Hence, various types of silane-kaolin interactions were generated due to KR high level of heterogeneity; this fact was somewhat sustained by the shoulder appearance for describing this specific degradation step. Here as well, TGA/ DTG results allowed KR thereof formulas to be calculated as follows: $Al_2Si_2O_5(OH)_4 \cdot (NH_2(CH_2)_3SiO_{1,5})_{0.37}$ for KR-APTS and $Al_2Si_2O_5(OH)_4 \cdot (NH_2(CH_2)_3Si(CH_3)_2O)_{0.53}$ for KR-APMS, respectively.

Fig 3 TGA curves and DTG inset of KR thereof; raw kaolin sample (KR), DMSO- intercalates (KR-DMSO), and organophilized samples with APMS and APTS (KR-APMS and KR-APTS).

The calculated chemical formulas of APTS and APMS kaolin thereof indicated similar orders of reactivity towards KR and KC kaolinite. These results also suggested that self-condensation of silane did not occur to a large extent, as confirmed by FTIR. Consequently, water absence and the competitive organophilization reaction at the kaolinite interface played an important role.

Structure. Fig 4 a and b depicts the infrared spectra of the KC thereof while **Fig S8**a and b (**ESI**) the infrared spectra of the KR thereof in the two specific wavenumber ranges (4000-2800 cm^{-1} and 1100-450 cm^{-1}, respectively). The bands at 3540 cm^{-1} and 3500 cm^{-1}, characteristic for DMSO-intercalated kaolinite, disappeared in the APTS and APMS-modified kaolinite samples. In addition, new bands at 2970 and 2930 cm^{-1} related to as. $\nu_{CH\ 3}$ and sym. ν_{CH2} vibrations of organosilane, reflected the presence of silane molecules in the APTS- and APMS-modified kaolinite samples. IR pattern of the OH stretching region for all silanized kaolin types was different from that of raw kaolinite.

Fig 4 The infrared spectra of KC, KC-DMSO, KC-APTS and KC-APMS in the 4000-2800 cm^{-1}**(a)** and 1100-450 cm^{-1}**(b)** specific wavenumber range.

The intensity decrease of the 3695 cm^{-1} band for KC thereof indicated a lower extent of accessible interlamellar hydroxyl groups. Furthermore, the intralamellar hydroxyl band was still

observed at 3620 cm^{-1} but significantly broader in the organophilized solids, indicating that the organophilization process has altered the environment of the platelets inner structure[33,41] Hence, grafting onto kaolinite surface was achieved.[44-46] As expected, the band at 938 cm^{-1} was quite discrete in KC-APTS and KC-APMS, relative to raw KC material, which confirmed the participation of interlamellar aluminol groups in the formation of new bonds with APTS and APMS.[29] A discrete presence of the 958 cm^{-1} band (aluminol-methyl interactions) was also noticed in both silane-intercalated kaolin types, validating the assumptions made previously at TGA i.e. the existence of some DMSO traces. Nevertheless, for APMS-intercalates some interference may come from the structural similarity of silane (two symmetrical methyl groups) with DMSO.

Similar changes were also obvious for KR derivatives, suggesting an efficient organophilization as well. The asymmetric and symmetric NH_2 stretching was more pronounced in KR thereof. The broad band between 3200 and 3500 cm^{-1}, reflected different environments for the amino groups involved in weak H-bonding with the interlamellar –OH surface (due to KR heterogeneity).[46] Additionally, DMSO was quantitatively removed from kaolinite interlayer space as indicated by the absence of aluminol-methyl interactions (958 cm^{-1}) in the spectra of organophilized - KR.

The XRD diffractograms of KC, KC-DMSO, KC-APTS and KC-APMS are shown in **Fig 5**a. The 10.9 Å d_{001} peak, characteristic for intercalated-DMSO, has been fully replaced in KC-APTS by one new reflection at 9.8 Å. The 9.8 Å basal spacing resulted from a flat monolayer arrangement of APTS molecules in the interlayer space of kaolinite.

Fig 5 X-ray diffraction patterns ($2\theta = 3\text{-}30^{O}$) of KC **(a)** and KR thereof **(b)**; raw kaolin samples (KC and KR), DMSO-intercalates (KC-DMSO and KR-DMSO), and organophilized samples with APMS and APTS (KC-APMS and KC-APTS, and KR-APMS and KR-APTS, respectively).

However, the 001 reflection is remarkably broad, indicating a heterogeneous intercalation process with low crystallinity and stacking order. Thus, the fact that APTS displays three possible grafting points led to different grafting reactions, including bridging of kaolinite platelets; implicitly, various interlayer distances were generated. The linking/bridging reaction, can also explain the contraction of the interlayer space relative to former DMSO-intercalates. A similar evolution was observed for the 3.7 Å peak (see KC-DMSO diffractogram), which became broader as well. Consequently, the low homogeneity and the fact that the organophilization process of kaolinite with APTS is generally uncontrollable, with some exceptions depict in the literature was confirmed. Moreover, the 001 reflection corresponding to non-intercalated kaolinite at 7.1 Å is relatively intense in KC-APTS, indicating that a high extent of kaolinite returned to the initial interlayer distance and remained non-intercalated after APTS organophilization. This supposition was also sustained by the similar trend of the 3.5 Å peak for which an intensity increase, relative to the DMSO-intercalate was registered. For KC-APMS a similar diffractogram to that of KC-DMSO was obtained. In this respect, the intensity of the 10.7 Å reflection characteristic for intercalated DMSO suggested that higher quantities of DMSO should have been present. Yet, the TGA and FTIR analyses indicated otherwise. Therefore, it is reasonable to assume that the peak at 10.7 Å belongs to KC-APMS intercalated structures where the aminopropyl group adopted a relatively flat orientation and the interlayer distance obtained previously by DMSO intercalation was not significantly affected. Some contributions to this conformation might have came from the nature of APMS molecules which can be found bonded on the inner surface of kaolinite by electrostatic interaction (the basic character of the -NH_2 might cause proton transfer from the acidic OH groups, resulting in an electrostatic interaction between single bond -NH_3^+ and surface O^{-},[35]).

Fig 6 Possible conformations of the organophilized kaolinite: **(a)** APTS molecules bridging kaolinite layers; **(b)** the APMS molecule adopting a flat orientation within the kaolinite interlayer space; **(c)** APTS molecules grafted at the edges and/or on the surface of the kaolinite layers.

More to this, the structural similarity of DMSO with APMS, both having two methyl groups which can interact with aluminol groups in a similar manner, may somehow influenced the little variance of the interlayer space. Unlike KC-APTS, only a small amount of kaolinite remained unmodified in APMS intercalates or returned to initial spatial arrangement, as indicated by the small peak at 7.1Å.[29]

The difference between the interlayer distances recorded for APMS and APTS after the organophilization reaction, can be explained through the ability of APTS to bridge the neighbouring kaolinite layers by their edges, thus obstructing APTS diffusion into the interlayer space (**Fig 6**a).[29] This bridging process was not possible for the monofunctional APMS molecules (**Fig 6**b), due to a single grafting point.[47] Consequently, the APMS intercalation process was more efficient and generated long-distance ordered structure (higher crystallinity degrees) of intercalated thereof as reflected by the constant interlayer distances (no staking).

The XRD analysis revealed rather different results for KR-APTS and KR-APMS intercalates (**Fig 5**b). After treating KR-DMSO with APTS, the resulting product displayed a more intense basal spacing at 7.1 Å, than KC-APTS, while the peak at 10.9 Å completely disappeared, suggesting that most kaolinite layers remained non-intercalated with APTS. The results also showed that the reaction exclusively occurred at the edges and/or on the surface of the kaolinite layers but not in the interlayer space. Contrary to KC-APTS, there are no silane molecules in the interlayer space of KR-APTS (**Fig 6**c).

For KR-APMS sample, quite surprisingly, no peak was registered at 10.9Å. Farmore, no new peaks with close basal spacing appeared instead while the peak at 7.1 Å remained at a very low intensity. These results have two possible

explanations: i) either the intercalation process occurred, but the basal peak was not visible in the studied region (3-30 θ); or ii) practical exfoliation occurred, excluding DMSO-intercalated kaolinite, which was still present in KR-APMS diffractogram. The exfoliation assumption was supported by the complete disappearance of the 3.7 Å peak, as well, which previous indicated the existence of intercalated structures. In can be also being noted here that obtaining exfoliated structures in the absence of solvents or in high defect kaolin samples is limited.

The ^{29}Si CP-MAS NMR (spectra of KC, KC-DMSO, KC-APMS and KC-APTS are shown in **Fig 7**) sustained the single-point grafting of APMS. The CP technique[48] was applied with a ramped ^{1}H-pulse starting at 100% power and decreasing until 50% during the contact time (3ms) in order to circumvent Hartmann-Hahn mismatches.[49,50]

Fig 7 Solid – state ^{29}Si CP-MAS spectra of the KC thereof; raw kaolin sample (KC), DMSO- intercalate (KC-DMSO), and organophilized samples with APMS and APTS (KC-APMS and KC-APTS).

To improve the resolution, a dipolar decoupling GT8 pulse sequence[51] was applied during the acquisition time. The peak at -90.4 ppm (Q^3 signal) in the ^{29}SiNMR spectrum of KC corresponded to the overlapping of two signals, assigned to the presence of two equal populated silicon sites in the tetrahedral sheets - highly characteristic to the unmodified kaolinite.[28,50,52]

For the KC-DMSO intercalate, the Q^3 signal is shifted to -91.8 ppm. The presence of this peak is the result of DMSO molecules intercalated with kaolinite sheets, as literature also suggested.[25,33,53] The ^{29}Si-NMR measurements further showed a shifting of the -91.8 ppm peak to -90.9 ppm, for KC-APTS[28] and KC-APMS. Such a low shift towards lower frequencies indicated that aminosilane molecules attached to the kaolinite aluminol groups presented little influence upon kaolinite silanol groups; this being a proof for the aminosilane grafting via Al–O–SiR bonds.[53]

The ^{29}Si-NMR data corroborated a bidentate [-60.2 for $RSi(OSi,Al)_2(OR')$ T^2] and and a tridentate [-67.5 ppm for $RSi(OSi,Al)_3$ sites T^3] fixation of APTS onto kaolinite facet with no contribution of monodentate fixation (T^1 sites).[1,28,53] In contrast, for the monofunctional silane (APMS) the ^{29}Si-NMR spectrum revealed only one peak at -8.4 ppm which corresponded to RR'_2SiOSi,Al sites M^1.[1] ^{29}Si NMR spectra of KR-APTS and KR-APMS (not shown) were similar to those of KC-APTS and KC-APMS, indicating similar grafting mechanisms

Experimental Details

Materials

Commercial kaolin clays from Romania and Brazil were employed in this study and used as received. The kaolin sample (KR) was obtained from the Aghires quarry (Cluj, Romania) and the two Amazonian kaolin samples KC and KD were kindly supplied by Dr C.O. Petter from the University of Porto Allegre (Brazil). **Table 2**, shows the chemical composition (as determined by EDAX analysis) of the kaolin from Romania (KR), as well as that of kaolin-C (KC) and kaolin–D (KD), both from Brazil. The effective kaolinite mineral within the two Brazilian rocks was above 95% for KD and above 97% for KC; the difference between the two Brazilian samples arise from the treatment steps which led to spherical compact particles (KD) and irregular confined particles of smaller size distribution (KC).

Dimethyl sulfoxide (DMSO, Sigma-Aldrich, 98%), 3-aminopropyl triethoxysilane (APTS, Fluka, 98%) and 3-aminopropyl dimethyl ethoxysilane (APMS, ABCR GmbH & Co.KG, 97%) were employed without further purification.

Table 2 Chemical composition of employed kaolin rocks (wt %)

Not.	SiO_2	Al_2O_3	TiO_2	Fe_2O_3	MnO	MgO	CaO	Na_2O	K_2O	P_2O_5
KR	42.40	48.70	2.56	3.30	-	0.73	0.98	0.59	0.65	-
KC	45.40	40.00	0.63	0.55	0.01	0.10	0.01	0.27	0.02	0.05
KD	44.90	39.10	1.60	1.10	0.01	0.15	0.01	0.30	0.02	0.05

DMSO intercalation and aminosilane grafting

A procedure similar to that used by Letaief and Detellier[25] for kaolin – DMSO intercalates (K-DMSO) was employed. Thus, 50 g of kaolin were dispersed (200 rpm) into a 12: 1 (*vol / vol*) DMSO: H_2O mixture (300 ml / 25 ml) under a nitrogen atmosphere at 80°C. After 10 days, the mixture was cooled down and the reaction product (K-DMSO) was recovered by centrifugation (6000 rpm) followed by washing with ethanol (2 x 250ml), at first, and then with isopropanol (2 x 250ml). Finally, the washed product was dried in an oven overnight (50°C). Subsequently, dry K-DMSO samples (1g) and the corresponding aminosilane (5 ml) were charged into a three necked- round bottom flask, under dry nitrogen atmosphere. Further on, the reaction mixture was heated (195°C) under constant magnetic stirring (200 rpm). After 48 h of reaction, the mixture was cooled down and the product (K-APTS or K-APMS) was recovered by centrifugation (6000 rpm). The solid was washed with toluene (3 x 10 ml) in order to remove the unreacted silane and dried overnight (105°C).

Characterization Methods

Morphological analyses were carried out on a XL30 Philips Scanning Electron Microscope, at 20 kV acceleration voltages (SE- secondary electrons) coupled with an elemental analyzer, EDAX module. FT IR spectra of samples were recorded on a Model 500 Nicolet FTIR instrument by averaging 32 scans with 4 cm^{-1} resolution, using the KBr pellet technique. The thermogravimetric analyses (TGA) were performed on a

Thermal Analysis SDT600 instrument, by heating samples of about 5-10 mg from room temperature to 1000°C at 10°C/min heating rate under nitrogen flow. X-ray diffractograms of modified kaolin were registered on a D5000 Siemens–Bruker diffractometer, equipped with a copper X-ray source (wavelength $\lambda=1.54.10^{-10}$ m; tension V=45 kV, intensity I=35mA), and with a monochromator eliminating Kβ radiation. The 2θ angle varied from 3° to 30° using a 35s step time and 0.04° step size. The solid-state ^{29}Si NMR spectra were obtained on a Bruker Avance-400 MHz NMR spectrometer operating at a ^{29}Si resonance frequency of 79,5 MHz and using a commercial Bruker double-bearing probe. About 100 mg of each sample was placed in zirconium dioxide rotors of 4 mm outer diameter and spun at a Magic Angle Spinning rate of 7 kHz. To obtain a good signal-to-noise ratio in ^{29}Si CPMAS experiment, 6000 scans were accumulated using a delay of 3s. The experiments were performed at ambient temperature. Chemical shifts were referenced to tetramethyl silane, whose resonance was set to 0 ppm.

Conclusions

Correlated results showed that both the intercalation and the organophilization processes were influenced by the morphology of raw kaolin, and, in equal measure, by the kaolin oxide structure and by the nature of aminosilane. The particle size and aggregation degree of KD kaolin led to a low intercalation yield of DMSO. The purity of kaolin samples had no significant influence upon the DMSO intercalation process. Thus, our paper also provides a new route for recycling the untreated rocks since the study proved that the heterogeneous oxide phases within the Romanian kaolin rock were inert to the intercalation processes. Yet, the ballast of KR played an important role for the organophilization reaction, especially for APTS grafting, where it somehow weakened the interlayer physical forces, allowing possible exfoliation processes. Organophilization reaction mechanisms differed for APMS and APTS, relative to the two kaolin types, partially due to APTS bridging, leading better yet to interpenetrated structures. The bridging reaction can also be the main cause for the low crystallinity degree in KC-APTS thereof that leads to difficulties in controlling the whole organophilization process. In contrast, the organophilization reaction with APMS was efficient because of the monofunctional nature of silane, which generated higher crystallinity structures with similar interlamellar space to that obtained for the KC-DMSO intercalate. Most importantly was the fact that KC organophilization with APMS led to single point grafted structures, making possible their further application as reinforcing agents. Additionally, the fact that exfoliation is still possible for these APMS-kaolinite intercalates opens new perspectives for other clay applications.

Acknowledgements

Financial support was given by the Romanian Ministry of Education and Research (via UEFISCDI), PCCA, through project SABIOM, number 114/2012; and by the the Ministry of European Funds: MANUNET. ERA-NET Project NASIPONAC number 7-074/2013 (via UEFISCDI) and Sectoral Operational Programme Human Resources Development 2007-2013, POSDRU/159/1.5/S/132395. The authors would like to thank for the solid-state ^{29}Si NMR spectra of Dr. eng. Fabio Ziarelli from Aix Marseille Université, Centrale Marseille, CNRS, Fédération des Sciences Chimiques FR 1739, F-13397 Marseille, France.

Notes and references

† Electronic Supplementary Information (ESI) available: Thermal analyses, and FTIR and XRD spectra of kaolin rocks and DMSO-kaolinite intercalates; FTIR of organophilised KR type. See DOI: 10.1039/c000000x/

1 N. Herrera, J. M. Letoffe, J. L. Putaux, L. David and E. Bourgeat-Lami, *Langmuir*, 2004, **20**, 1564-1571.
2 A. L. Radu, C. Damian, V. Fruth, T. V. Iordache, A. Zaharia, H. Iovu and A. Sarbu, *Micropor. Mesopor. Mat.*, 2014, **198**, 281-290.
3 A. Lungu, F. X. Perrin, L. Belec, A. Sarbu and M. Teodorescu, *Appl. Clay Sci..,* 2012, **62-63**, 63-69.
4 G. W. Brindley and J. LeMaitre in *Chemistry of Clays and Clay Minerals, Monograph 6* (ed. A.C.D. Newman), Mineralogical Society, Longman & Scientific Technical, Essex, 1987, pp. 319-370.
5 R. Ianchis, M. C. Corobea, D. Donescu, I. D. Rosca, L. O. Cinteza, C. L. Nistor, E. Vasile, A. Marin and S. Preda, *J. Nanopart. Res.*, 2012, **14**, 1214-1233.
6 A. Zaharia, A. Sarbu, A. L. Radu, K. Jankova, A. Daugaard, S. Hvilsted, F. X. Perrin, M. Teodorescu, C. Munteanu and V. Fruth-Oprisan, *Appl. Clay Sci.*, 2015, **103**, 46-54.
7 S. Wang, Z. Ahmad and J. E. Mark, *Chem. Mater.*, 1994, **6**, 943-946.
8 J. P. Chen, Z. Ahmad, S. H. Wang, J. E. Mark and F. E. Arnold, *ACS Symposium Series*, 1995, **585**, 297-306.
9 M. I. Sarwar, S. Zulfiqar and Z. Ahmad, *Colloid Polym. Sci.*, 2007, **285**, 1733-1739.
10 F. Babonneau, *Polyhedron*, 1994, **13**, 1123-1130.
11 M. I. Sarwar, S. Zulfiqar and Z. Ahmad, *J. Sol-Gel Sci. Techn.*, 2008, **45**, 89-95.
12 B. K. G. Theng, Elsevier, New York, 1979.
13 C. C. Harvey and G. Lagaly in *Handbook of Clay Science, Developments in Clay Science*, 1 (Eds: F. Bergaya, B.K.G. Theng, G. Lagaly), Elsevier, 2006.
14 R. Ianchis, L. O. Cinteza, D. Donescu, C. Petcu, M. C. Corobea, R. Somoghi, M. Ghiurea and C. Spataru, *Appl. Clay Sci.*, 2011, **52**, 96-103.
15 N. A. Akhtar and W. E. Worral, *Brit. Ceram. Trans. J.*, 1975, **74**, 105-111.
16 Y. Li, D. Sun, X. Pan and B. Zhang, *Clay Clay Miner.*, 2009, **57**, 779-786.
17 C. Chakraborty, P. K. Sukul, K. Dana and S. Malik, *Ind. Eng. Chem. Res.*, 2013, **52**, 6722-6730.
18 J. E. Gardolinski, L. C. M. Carrera, M. P. Cantão and F. Wypych, *J. Mater. Sci.*, 2000, **35**, 3113-3119.
19 A. Matsumura, Y. Komori, T. Itagaki, Y. Sugahara and K. Kuroda, *B. Chem. Soc. JPN*, 2001, **74**, 1153-1158.

20 Y. Komori, Y. Sugahara and K. Kuroda, *Appl. Clay Sci.*, 1999, **15**, 241-252.
21 J. E. Gardolinski and G. Lagaly, *Clay Miner.*, 2005, **40**, 547-556.
22 E. H. de Faria, O. J. Lima, K. J. Ciuffi, E. J. Nassar, M. A. Vicente, R. Trujillano and P. S. Calefi, *J. Colloid Interf. Sci.*, 2009, **335**, 210-215.
23 S. Letaief and C. Detellier, *Chem Commun*, 2007, **1**, 2613-2615.
24 S. Letaief, I. K. Tonle, T. Diaco and C. Detellier, *Appl. Clay Sci.*, 2008, **42**, 95-101.
25 S. Letaief and C. Detellier, *J. Mater. Chem.*, 2005, **15**, 4734-4740.
26 H. He, Q. Tao, J. Zhu, P. Yuan, W. Shen, S. Yang, *Appl. Clay Sci.*, 2013, **71**, 15–20.
27 S. S. Gupta and K. G. Bhattacharyy, *Phys. Chem. Chem. Phys.*, 2012,**14**, 6698-6723.
28 I. K. Tonlé, T. Diaco, E. Ngameni and C. Detellier, *Chem. Mater.*, 2007, **19**, 6629-6636.
29 L. R. Avila, E. H. de Faria, K. J. Ciuffi, E. J. Nassar, P. S. Calefi, M. A. Vicente and R. Trujillano, *J. Colloid Interf. Sci.*, 2010, **341**, 186-193.
30 S. Nakagaki, F. L. Benedito and F. Wypych, *J. Mol. Catal. A-Chem.*, 2004, **217**, 121-131.
31 A. D. Gianni, E. Amerio, O. Monticelli and R. Bongiovanni, *Appl. Clay Sci.*, 2008, **42**, 116-124.
32 R. L. Frost, J. Kloprogge, S. C. Russell and J. L. Szetu, *Thermochim. Acta*, 1999, **329**, 47-56.
33 T. A. Elboki and C. Detellier, *J. Colloid. Interf. Sci.*, 2008, **323**, 338-348.
34 J. D. Russel, M. J. Wilson, Chapman and Hall Ed., New York, 1987, pp. 133-173.
35 S. -Q. Yang, P. Yuan, H. -P. He, Z. -H. Qin, Q. Zhou, J. -Xi Zhu and D. Liu, *Appl. Clay Sci.*, 2012, **62-63**, 8-14.
36 M. Castellano, A. Turturro, P. Riani, T. Montanari, E. Finocchio, G. Ramis and G. Busca, *Appl. Clay Sci.*, 2010, **48**, 446-454.
37 C. S. Manju, V. Narayanan Nair and M. Lalithambika, *Clay Clay Miner.*, 2001, **49**, 355-369.
38 D. Sun, B. Li, Y. Li, C. Yu, B. Zhang and H. Fei, *Mater. Res. Bull.*, 2011, **46**, 101-104.
39 J. Kristóf, R. L. Frost, J. T. Kloprogge, E. Horváth and M. Gábor, *J. Therm. Anal. Calorim.*, 1999, **56**, 885-891.
40 M. L. Jackson and F. H. Abdel-Kader, *Clay Clay Miner.*, 1978, **26**, 81-87.
41 R. L. Frost, J. Kristof, G. N. Paroz and J. T. Kloprogge, *J. Phys. Chem. B*, 1998, **102**, 8519-8532.
42 E. Horvath, J. Kristof and R. L. Frost, *Appl. Spectrosc. Rev.*, 2010, **45**, 130-147.
43 M. J. Duer, J. Rocha and J. Klinowski, *J. Am. Chem. Soc.*, 1992, **114**, 6867-6874.
44 M. Valášková, M. Rieder, V. Matějka, P. Čapková and A. Slíva, *Appl. Clay Sci.*, 2007, **35**, 108-111.
45 R. L. Frost, D. A. Lack, G. N. Paroz and T. H. Tran, *Clay Clay Miner.*, 1999, **47**, 297-303.
46 S. Letaief, T. A. Elboki and C. Detellier, *J. Colloid Interf. Sci.*, 2006, **302**, 254-258.
47 J. G. Thompson and P. F. Barron, *Clay Clay Miner.*, 1987, **35**, 38-42.
48 J. Schaefer and E. O. R. Stejskal, *J. Am. Chem. Soc.*, 1976, , 1031-1032.
49 O. B. Peersen, X. Wu, I. Kustanovich and S. O. Smith, *J. Magn. Reson.*, 1993, **104**, 334-339.
50 R. L. Cook, C. H. Langford, R. Yamdagni and C. M. Preston, *Anal. Chem.*, 1996, **68**, 3979-3986.
51 G. Gerbaud, F. Ziarelli and S. Caldarelli, *Chem. Phys. Lett.*, 2003, **377**, 1-5.
52 T. A. Elboki and C. Detellier, *J. Phys. Chem. Solids*, 2006, **67**, 950-955.
53 E. Moretti, L. Storaro, G. Chessa, A. Talon, E. Callone, K. J. Mueller, F. Enrichi and M. Lenarda, *J. Colloid Interf. Sci.*, 2012, **375**, 112-117.

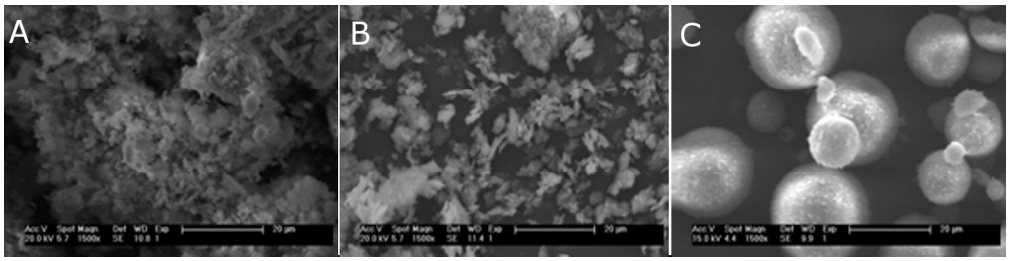

Fig 1 Shape and morphology of the raw kaolin samples KR (A), KC (B) and KD (C).
164x41mm (300 x 300 DPI)

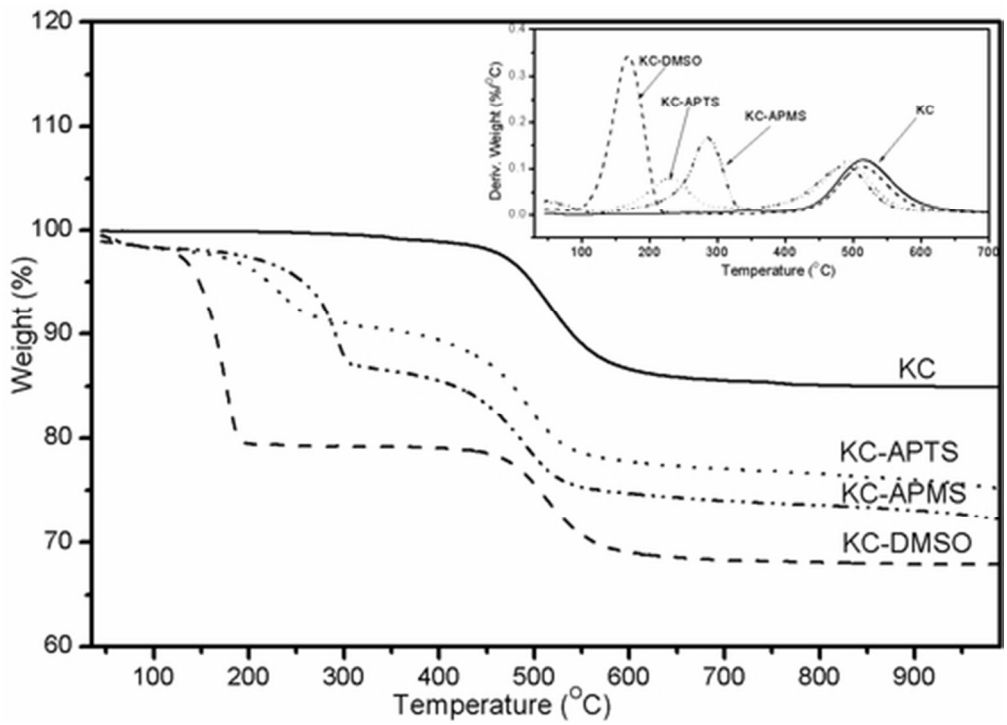

Fig 2 TGA curves and DTG inset of KC thereof; raw kaolin sample (KC), DMSO-intercalate (KC-DMSO), and organophilized samples with APMS and APTS (KC-APMS and KC-APTS).
43x30mm (300 x 300 DPI)

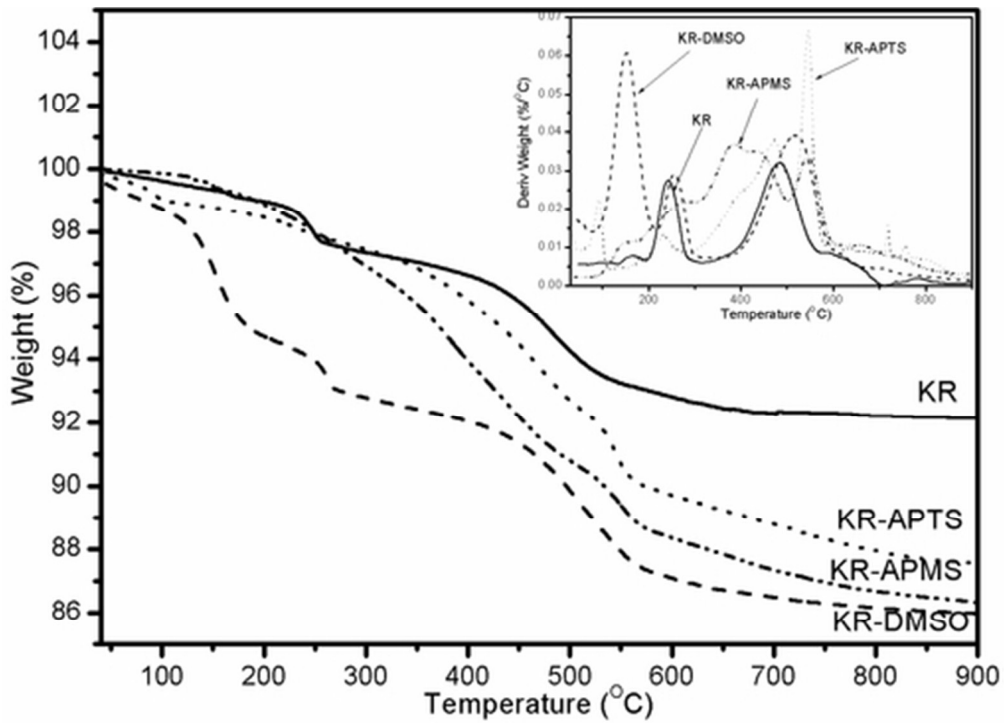

Fig 3 TGA curves and DTG inset of KR thereof; raw kaolin sample (KR), DMSO- intercalate (KR-DMSO), and organophilized samples with APMS and APTS (KR-APMS and KR-APTS).
42x30mm (300 x 300 DPI)

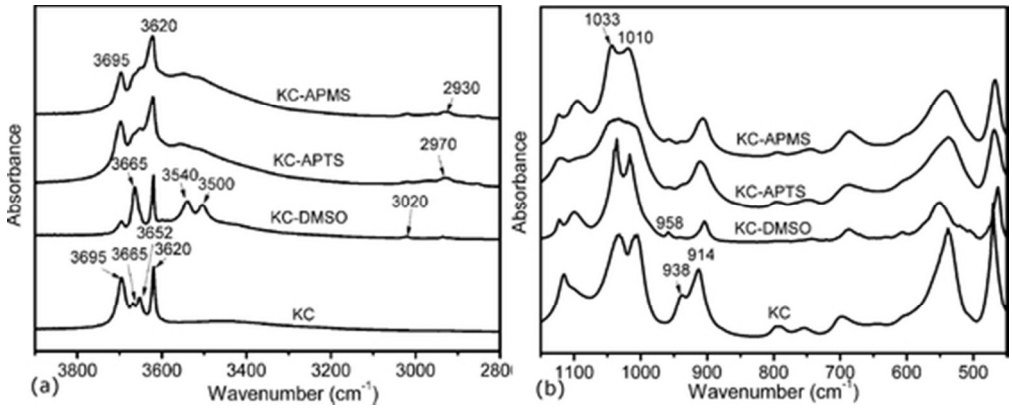

Fig 4 The infrared spectra of KC, KC-DMSO, KC-APTS and KC-APMS in the 4000-2800 cm-1(a) and 1100-450 cm-1(b) specific wavenumber range.
46x18mm (300 x 300 DPI)

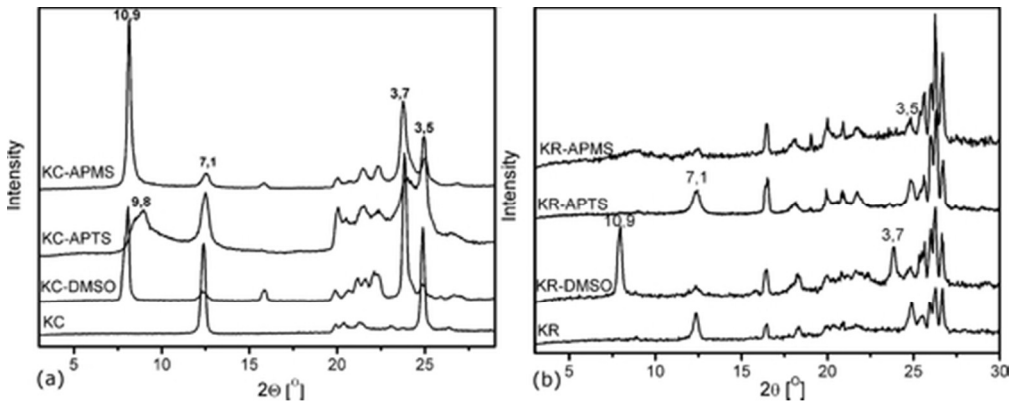

Fig 5 X-ray diffraction patterns (2θ = 3-30O) of KC (a) and KR thereof (b); raw kaolin samples (KC and KR), DMSO- intercalates (KC-DMSO and KR-DMSO), and organophilized samples with APMS and APTS (KC-APMS and KC-APTS, and KR-APMS and KR-APTS, respectively).
46x18mm (300 x 300 DPI)

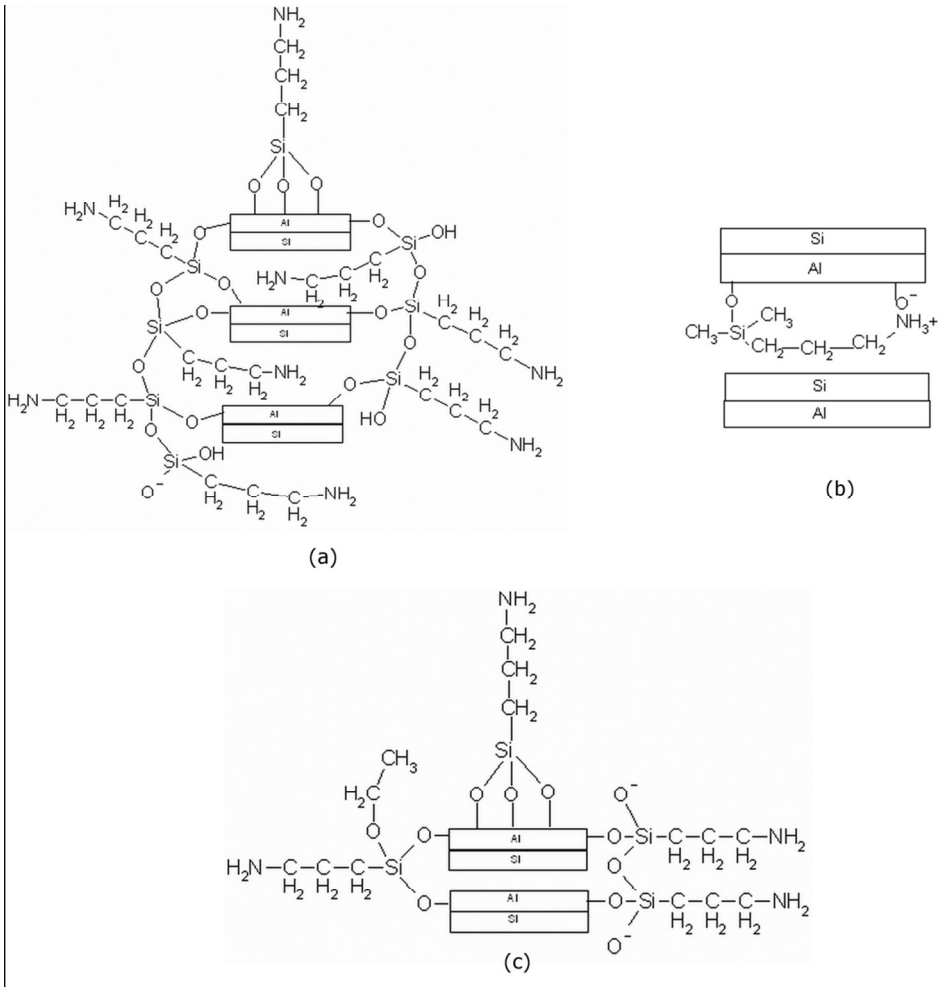

Fig 6 Possible conformations of the organophilized kaolinite: (a) APTS molecules bridging kaolinite layers; (b) the APMS molecule adopting a flat orientation within the kaolinite interlayer space; (c) APTS molecules grafted at the edges and/or on the surface of the kaolinite layers
104x102mm (300 x 300 DPI)

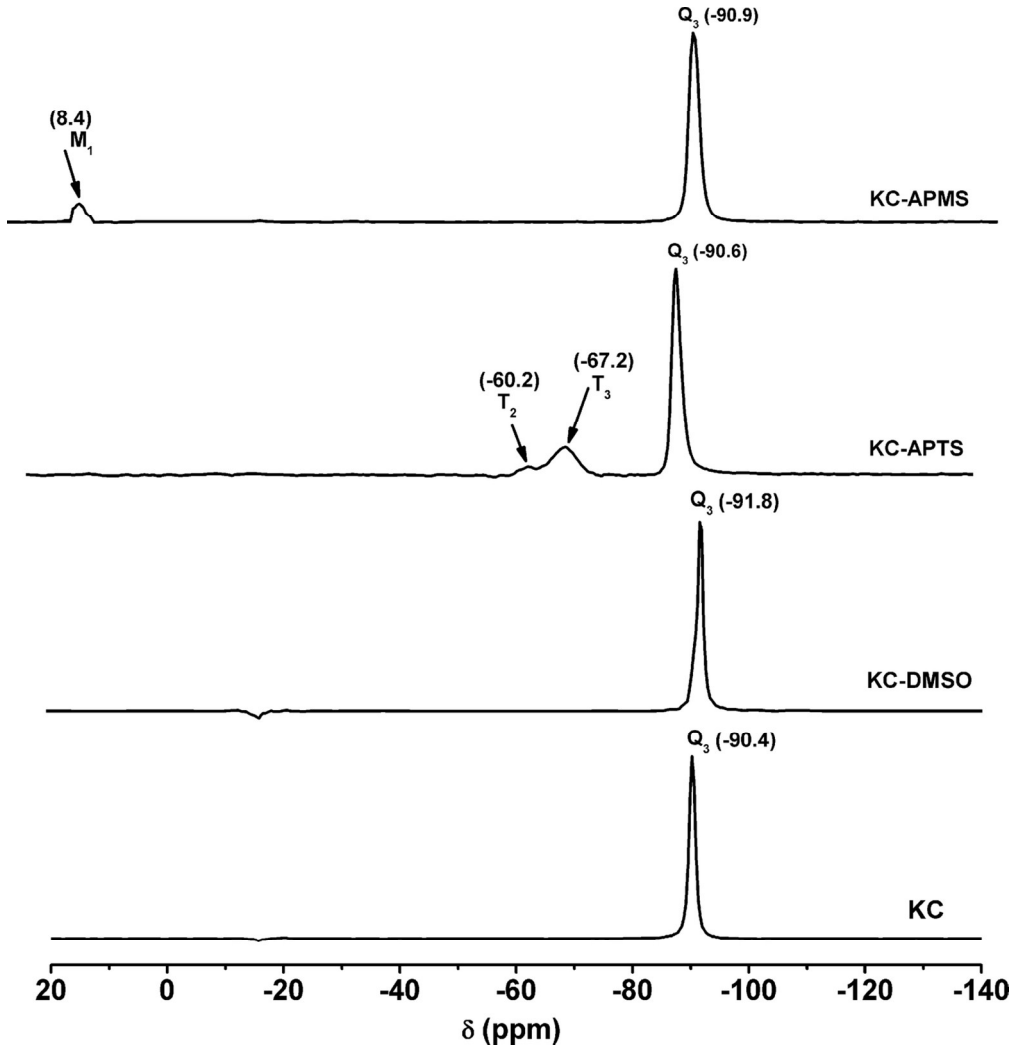

Fig 7 Solid – state 29Si CP-MAS spectra of the KC thereof; raw kaolin sample (KC), DMSO- intercalate (KC-DMSO), and organophilized samples with APMS and APTS (KC-APMS and KC-APTS).
124x128mm (300 x 300 DPI)